

Corrosion Behavior of A High Purity Iron Surface-Modified Nitrogen Ion Implantation

Hee-Jae-Kim* and Robert F. Hochman**

**Department of Weapons Engineering
Korea Military Academy*

***School of Materials Engineering
Georgia Institute of Technology
Atlanta, GA 30332 U.S.A.*

ABSTRACT

The corrosion behavior of a high purity iron implanted with nitrogen ions was studied as a model substrate to avoid the complications which alloy additions would introduce. The composition and structure of the implanted layer were examined to determine the mechanisms by which nitrogen ion implantation affected the corrosion characteristics of the substrate. Results show significant increase of corrosion resistance by implantation with a higher dosage at higher accelerating voltage than a lower dosage at lower accelerating voltage. It is hypothesized that ion implantation may reduce the crystallographic roughness and provide a homogeneous surface for the passive film formation, and that the enrichment of implanted species may tie up the iron in thermodynamically stable compounds.

1. INTRODUCTION

Modification of the corrosion behavior of metals and alloys by ion implantation has received increased attention during the past several years. The feasibility of changing the alloy composition and microstructure of the near-surface region may be useful in improving corrosion resistance by reducing the rate of anodic oxidation and/or the cathodic reduction. Since the near-surface composition is not limited by the equilibrium solubility of the implanted element, novel alloys can be produced [1]. There is no discrete interface between the modi-

fied layer and the substrate, and consequently, there is no adhesion problem as is the case with other process such as electro-plating or ion plating.

The implantation process can enhance passive oxide formation and shows an improvement in the corrosion resistance during short-term electrochemical testing [2]. In particular, nitrogen ion implantation into iron and steels has been observed to improve such technologically important properties as corrosion resistance and the resistance to wear and fatigue [3-5]. However, the many ambiguities apparent in

the literature indicate the complex nature of ion implantation processes and the materials resulting from its use. In addition, the mechanism which produces this change in corrosion characteristics is still not understood.

In present work, a high purity iron was chosen as a model substrate to avoid the complications which impurities and alloy additions would introduce. The composition and structure of an iron surface were modified by nitrogen ion implantation with two different conditions: (a) a lower ion dosage at lower accelerating voltage and (b) a higher ion dosage at higher accelerating voltage. The corrosion properties of the samples were evaluated to determine the mechanisms by which the ion implantation affected the corrosion behavior of the substrate.

2. EXPERIMENTAL PROCEDURES

The substrate material used in this study was vacuum-melted iron of 99.9985 % purity. To produce test specimens, the as-received rod was machined to 9.5 mm diameter and cut into discs 2.5 mm thick. One side of each disc was wet-ground progressively with finer grit and metallurgically polished with one micron diamond paste. After Polishing, specimens were ultrasonically cleaned in a detergent. The polished surfaces were implanted with nitrogen ions under two different conditions: (1) a fluence of 1×10^{17} ions cm^{-2} at 50 KeV, and (2) a fluence of 2.5×10^{17} ions cm^{-2} at 100 KeV. The vacuum in the implantation chamber was less than 5×10^{-6} torr during implantation.

Auger profiles as a function of depth were made in a PHI Model 590 Scanning Auger Microprobe. Profiling was achieved by sputtering with purified argon gas using a primary ion energy of 2 or 5 KeV and an ion beam size of 200 microns in an ultra high vacuum system with

a vacuum of approximately 10^{-10} torr. Elemental compositions were determined from the Auger electron spectroscopy (AES) peak-to-peak heights of the derivative spectra of each element and their relative sensitivity [6]. The depth produced by sputtering was determined by measurement using a Ta_2O_5 standard. This allowed the relationship between sputter time and thickness of the layer removed (sputter rate) to be determined. The sputter rate was assumed to be a constant. The probable error in determining the elemental concentration and sputter rate was about 20 percent.

X-ray photoelectron spectroscopy was performed to study the structure and chemical state of the elements in the surface layer of the implanted specimen. X-ray photoelectron spectra of the specimens were taken on a Physical Electronic Model 560 ESCA/SAM Electron Spectrometer. The photoelectron spectra of each prominent element was obtained: (1) from the as-implanted surface, and (2) from the surface after argon ion etching to a depth of 40 Å. A small amount of sputtering was performed to remove carbonaceous contaminants on the sample surfaces. The measured electron binding energies were calibrated by reference to an adventitious carbon standard 1s line which is 284.6 eV [7]. Probable error in calibration and measurement of the binding energy at the peak maximum is ± 0.2 eV.

The surface structures of the unimplanted and implanted samples were examined and characterized by transmission electron microscopy (TEM). Thin foils were electropolished on one side without perforation, using a solution of 5 percent perchloric acid and 95 percent acetic acid at 10 to 13°C. The electropolishing voltage varied from 35 to 45 volts. The thus polished foils were then implanted on the poli-

shed side. The implanted samples were then electropolished from the unimplanted side of the foil to produce electron-transparent thin areas. The completed thin foils were examined in a JEOL JEM-100C electron microscope at an operating voltage of 100 KeV.

The effect of nitrogen ion implantation on the corrosion behavior of the materials was investigated using a potentiodynamic polarization technique. Polarization experiments were performed in a deaerated 1N H_2SO_4 aqueous solution and a deaerated 0.1M NaCl aqueous solution. The solution was agitated during testing with a magnetic stirrer. All potentials were monitored with respect to a saturated calomel electrode (SCE) at 25°C. The voltage was scanned at 1 mV sec⁻¹ starting 300 mV below the open circuit potential in the noble direction.

Following the potentiodynamic polarization tests, the corroded surfaces of the tested samples were examined in scanning electron microscope operated at 20 KeV to evaluate the morphology of the corroded surfaces, shape and size of corrosion products, and phases present in the surfaces.

3. RESULTS AND DISCUSSIONS

Figure 1 is an Auger depth profile of implanted nitrogen in the near-surface region of iron implanted with a fluence of 1×10^{17} nitrogen ions cm⁻² at 50 KeV. A Gaussian distribution of nitrogen skewed toward the surface is evident. The maximum concentration of nitrogen was about 25 atomic percent at 500 Å. The total projected range was about 1400 Å. The skewed effect toward the surface was less noticeable in the iron implanted with a fluence of 2.5×10^{17} nitrogen ions cm⁻² at 100 KeV as shown in Figure 2. The maximum nitrogen

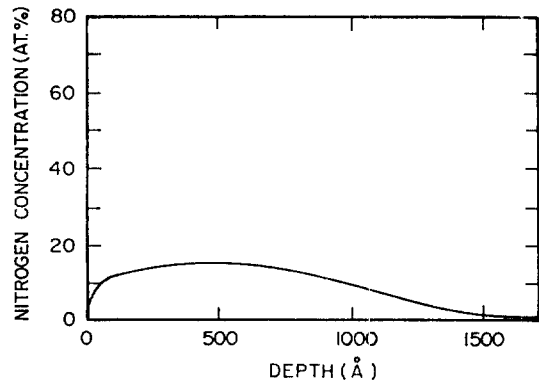


Figure. 1. AES Depth Profile of Nitrogen in Iron Implanted with 1×10^{17} Nitrogen Ions cm⁻² at 50 KeV.

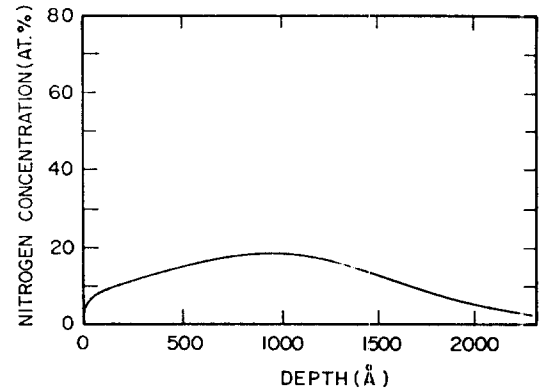


Figure. 2. AES Depth Profile of Nitrogen in Iron Implanted with 2.5×10^{17} Nitrogen Ions cm⁻² at 100 KeV.

concentration was about 18 atomic percent and located at about 1100Å beneath the surface. The total projected range was about 2400 Å.

Ion implantation with the higher accelerating voltage and the higher total dosage produced a greater penetration and a higher maximum concentration of implanted ions for a given substrate than did the lower accelerating voltage and lower total dosage. The total penetration depth and maximum nitrogen concentration are consistent with the prediction of LSS theory [8].

The photoelectron spectra of N 1s electrons from nitrogen implanted iron are given in Figures 3 and 4. The N 1s peak for iron implanted with a fluence of 1×10^{17} nitrogen ions cm^{-2} at 50 KeV had a maximum of about 397.2 eV and was identified as an iron nitride [9]. After argon ion etching to a depth of about 40 Å, the binding energy of the N 1s spectrum was found to be 397.5 eV. This binding energy can be attributed to an iron nitride state of nitrogen [9]. For iron implanted with a fluence of 2.5×10^{17} nitrogen ions cm^{-2} at 100 KeV, a broad range of N 1s peak was observed in the range of 396.3-397.9 eV as shown in Figure 4. This peak might be composed of two peaks at about 396.3 and 397.8 eV, which could be attributed to nitrides [9]. After argon ion etching to a depth of about 40 Å, the N 1s electron peak showed a single sharp

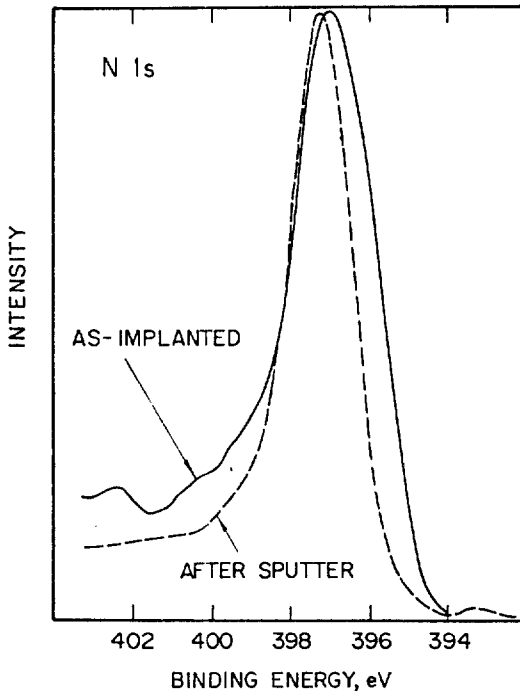


Figure 3. X-ray Photoelectron Spectra of N 1s Electrons in Iron Implanted with 1×10^{17} Nitrogen Ions cm^{-2} at 50 KeV.

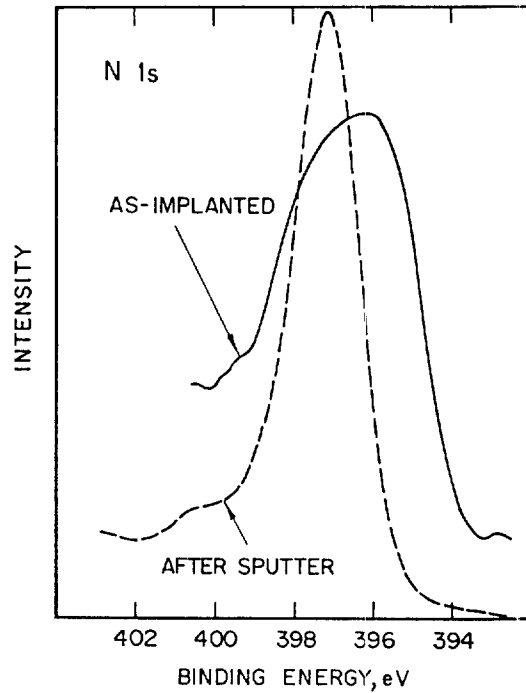


Figure 4. X-ray Photoelectron Spectra of N 1s Electrons in Iron Implanted with 2.5×10^{17} Nitrogen Ions cm^{-2} at 100 KeV.

peak, which is characteristic of an iron nitride.

Figure 5 shows the TEM micrograph of as-received iron. A large density of dislocations was present in the structure since the as-received iron still retains a fair amount of cold work from processing. Implantation with a fluence of 1×10^{17} nitrogen ions cm^{-2} at 50 KeV introduced a large density of dislocations in the structure as shown in Figure 6. A selected area diffraction pattern of the structure confirmed the presence of a single phase, ferritic structure without additional spots. Figure 7 shows the TEM micrograph of iron implanted with a fluence of 2.5×10^{17} nitrogen ions cm^{-2} at 100 KeV. A high density of dislocations were well distributed in the structure of a single phase, ferritic structure.

However, TEM studies of as-implanted iron

did not reveal any secondary phases. Only a structure with a high density of tangled dislocations was observed. This is probably related to the effects of implantation temperature where any precipitates produced at low implantation temperature (below 200°C) may not be large enough to be detected by TEM. Any small volume fraction of ultra fine precipitates may be undetectable with electron diffraction.



Figure 5. Transmission Electron Micrograph of As-received Iron.



Figure 7. Transmission Electron Micrograph of Iron Implanted with 2.5×10^{17} Nitrogen Ions cm^{-2} at 100 KeV.

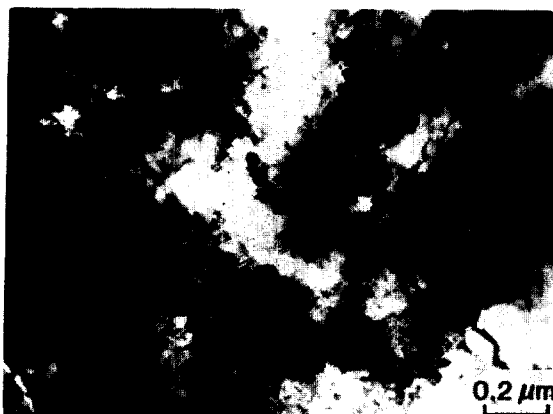


Figure 6. Transmission Electron Micrograph of Iron Implanted with 1×10^{17} Nitrogen Ions cm^{-2} at 50 KeV.

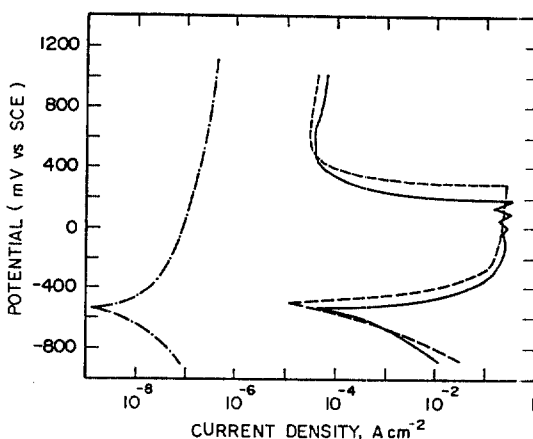


Figure 8. Potentiodynamic Polarization Curves of Iron in Deaerated 1N H_2SO_4 Solution Unimplanted (—), Implanted with 1×10^{17} Nitrogen Ions cm^{-2} at 50 KeV (---), and Implanted with 2.5×10^{17} Nitrogen Ions cm^{-2} at 100 KeV. (· · ·)

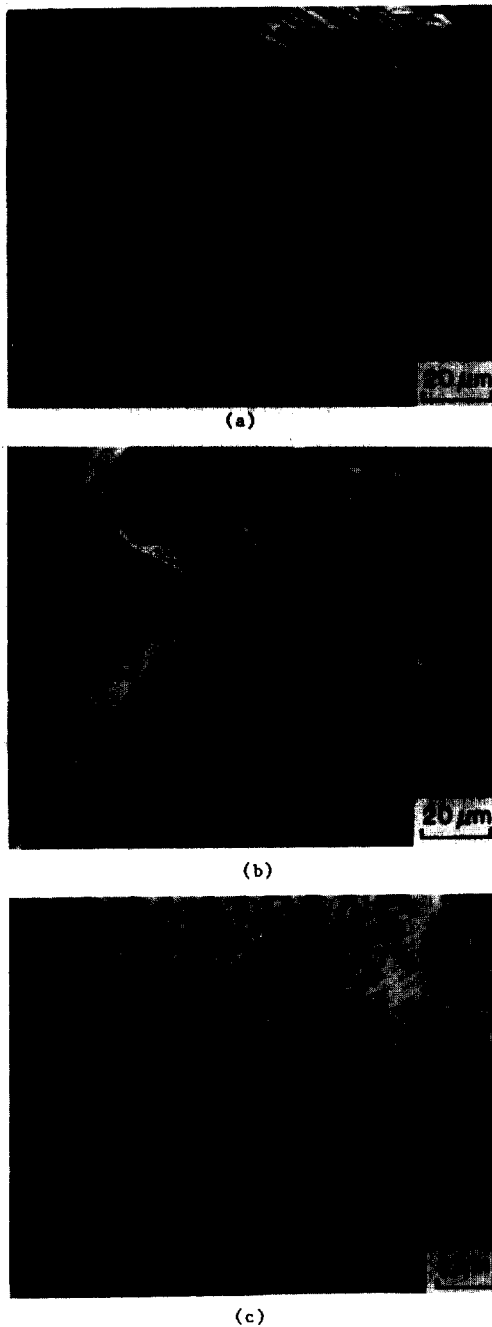


Figure. 9. SEM Micrographs of Iron Corroded in Deaerated 1N H₂SO₄ Aqueous Solution: (a) Unimplanted, (b) Implanted with 1 × 10¹⁷ Nitrogen ions cm⁻² at 50 KeV, and (c) Implanted with 2.5 × 10¹⁷ Nitrogen ions cm⁻² at 100 KeV.

nitrogen ions cm⁻² at 100 KeV resulted in a significant reduction in the current density across the entire potential range tested. The corrosion rate at the open circuit potential was reduced by four orders of magnitude, but the open circuit potential was essentially the same. No breakdown potential was observed in the test range studied.

Figure 9 shows the SEM micrographs of surfaces corroded during research conducted in this study. Implantation with a fluence of 1 × 10¹⁷ nitrogen ions cm⁻² at 50 KeV produced the same corrosion morphology than unimplanted iron displayed, although the corroded grain surfaces were smoother than for the unimplanted iron. Implantation with a fluence of 2.5 × 10¹⁷ nitrogen ions cm⁻² at 100 KeV produced a uniform but mottled attack on the surface without defined grain boundaries.

Figure 10 shows the potentiodynamic polarization curves of unimplanted and nitrogen implanted irons tested in deaerated 0.1M NaCl solutions. Implantation with a fluence of 1 × 10¹⁷

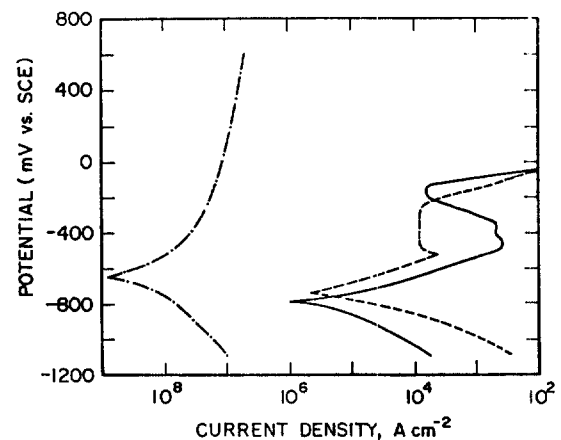
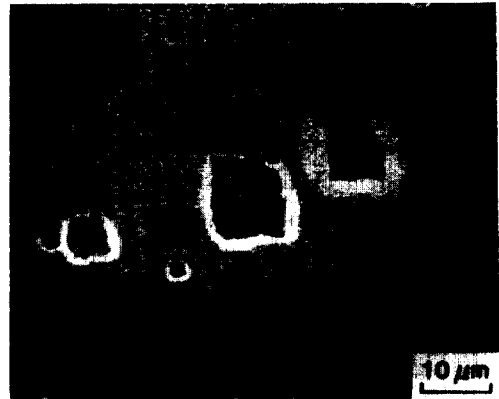


Figure. 10. Potentiodynamic Polarization Curves of Iron in Deaerated 0.1M NaCl Solution: Unimplanted (—), Implanted with 1 × 10¹⁷ Nitrogen ions cm⁻² at 50 KeV (---), and Implanted with 2.5 × 10¹⁷ Nitrogen ions cm⁻² at 100 KeV (-.-)

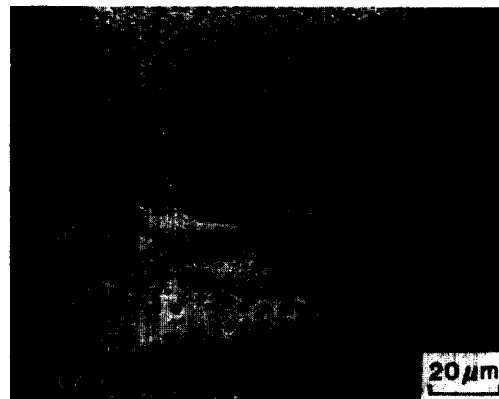
nitrogen ions cm^{-2} at 50 KeV resulted in lower pitting potential than that of unimplanted iron. However, implantation with a fluence of 2.5×10^{17} nitrogen ions cm^{-2} at 100 KeV showed no observable pitting potential in the range tested. The current densities at all potentials were reduced. Nitrogen implantation elevated the open circuit potential of the iron for both implanted conditions, but most significantly for the 100 KeV and 2.5×10^{17} dose implantation. SEM micrographs of the corroded surfaces are shown in Figure 11. Localized pitting with a large number of small pits (approximately 1-2 microns in diameter) was observed on the surface implanted with lower voltage and fluence. Pits produced on the surface implanted with the higher voltage and fluence appeared to be easily repassivated as shown in Figure 11(c).

A nitrogen ion dose of 2.5×10^{17} ions cm^{-2} implanted at an accelerating voltage of 100 KeV produced a significant increase in both general and pitting corrosion resistance of iron. A lower nitrogen dose of 1×10^{17} ions cm^{-2} implanted at an accelerating voltage of 50 KeV showed little or no improvement in corrosion resistance in deaerated 1N H_2SO_4 aqueous solution, and a tendency for increased pitting in deaerated 0.1M NaCl aqueous solution.

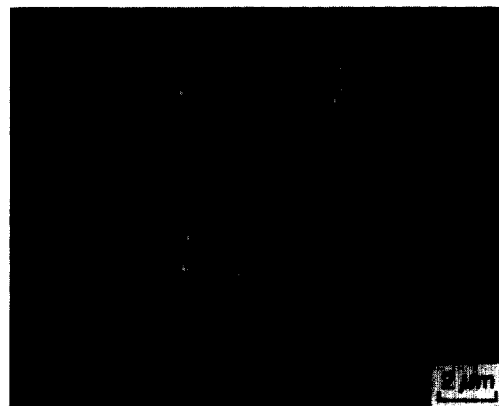
Ion implantation may reduce the crystallographic roughness and provide a more homogeneous surface for the formation of a passive film than the normal crystalline state, or the implanted layer itself may act in a part as a preformed protective layer. One would also expect adhesion between the implanted layer and the passive surface to be better. It is borne out by the enhanced resistance produced by the higher dosage and higher energy nitrogen implantation. However, a lower dosage and lower energy implantation of nitrogen does not produce suffi-



(a)



(b)



(c)

Figure. 11. SEM Micrographs of Iron Corroded in Deaerated 0.1M NaCl Aqueous Solution: (a) Unimplanted, (b) Implanted with 1×10^{17} Nitrogen ions cm^{-2} at 50 KeV, and (c) Implanted with 2.5×10^{17} Nitrogen ions cm^{-2} at 100 KeV.

cient changes in the iron surface to provide the conditions necessary to form a protective film.

The pitting resistance of the implanted iron in deaerated 0.1M NaCl solution is even more dependent on the uniformity and stability of the modified surface layer. The possible repassivation of pits in the implanted surface may be attributed to the presence of the high nitrogen concentration along the lines of the model suggested by Hartline [10] where nitrogen in the implanted iron consumes protons when it dissolves in a pit resulting from the formation of NH_3^+ ions. This prevents the lowering of PH in the pit and provides an environment for repassivation before the pit grows larger. This is also in keeping with the observation that an iron surface implanted with a lower dosage and at a lower accelerating voltage may not be able to provide sufficient nitrogen to sustain such repassivation.

The improvement of corrosion resistance of iron may also be attributed to the nitrides present in the implanted surface layer (found in the XPS study) similar to the conditions achieved for gas nitrides [11]. Nitrogen implantation into iron shifts the open circuit potential to a more noble direction (Figures 8 and 9). The enhanced nobility of the iron surface, although of secondary importance to the previously discussed factors, may aid the overall corrosion resistance of the implanted iron surface.

In summary, the improvement in the experimental corrosion resistance observed may be attributed to two effects produced by implantation. One is the enrichment of the surface in nitrogen, which has been shown to reduce corrosion, and the other is the homogeneous (but reactive) surface conditions which result in an improved passive layer.

General Hypotheses for the Reduced Corrosion Found in This Study

Two interrelated mechanisms are hypothesized from the observed improvement in corrosion resistance of implanted iron. First, a heavily disturbed surface layer produced by iron implantation should be more reactive than untreated surface layer due to the radiation damage. However, this modified layer can be considered more homogeneous and reactive. Hence, a passive film can form rapidly in a corrosive environment, and this film may be postulated to be more adherent since no epitaxial relations to the substrate are necessary. This is very much keeping with the observation of the highly disturbed surface produced by the higher energy and higher dose nitrogen implantation.

The second facet of the hypothesis for improved corrosion resistance of nitrogen implanted iron is nitrogen surface enrichment which may tie up the iron in thermodynamically stable compounds reducing the amount which may go into solution.

4. CONCLUSIONS

1. Nitrogen ion implantation into the high purity iron introduced a large density of tangled dislocations in the implanted structure and ultra fine iron nitrides.

2. Nitrogen ion implantation into iron with a higher dosage and voltage (2.5×10^{17} ions cm^{-2} and 100 KeV) significantly increases corrosion resistance in deaerated 1N H_2SO_4 and 0.1M NaCl aqueous solutions compared to the high purity iron and the iron implanted with lower dosage and voltage (1×10^{17} ions cm^{-2} and 50 KeV).

5. REFERENCES

1. A. Perez and R. Coussement eds., *Site Characterization and Aggregation Implanted Atoms in Materials*, Plenum Press, New York, (1980).
2. V. Ashworth, W.A. Grant, R.P.M. Procter, and T.C. Wellington, *corros. Sci.*, **16**, 393 (1976).
3. Wen-Wei Hu, C.R. Clayton, and H. Herman, *Scripta Met.*, **12**, 697 (1978).
4. W.C. Oliver, R. Hutchings, and J.B. Pethica, *Metal. Trans.*, **15A**, 2221 (1984).
5. P.L. Bonora, M. Bassoli, G. Cerisola, P.L. de Anna, S. Lo Russo, P. Mazzololi, B. Tiveron, I. Scotonic, C. Tosello, and A. Bernard, *Nucl. Instr. and Meth.*, **182/183**, 1001 (1981).
6. L.E. Davis, N.C. MacDonald, P.W. Palmberg, G.E. Riach, and R.E. Weber eds., *Handbook of Auger Electron Spectroscopy*, 2nd ed., Physical Electronic Industries Inc., Eden Prairie, MN (1976), p. 9.
7. C.D. Wagner, W.M. Riggs, L.E. Davis, J.G. Moulder, and G.E. Muilenberg, *Handbook of X-ray Photoelectron Spectroscopy*, Perkin Elmer Corp., Eden Prairie, MN (1979), p. 17.
8. J. Lindhard, M. Scharff, and H.E. Schiott, *Kgl. Danske Vid. Selsk., Mat. Fys. Medd.*, **33**, No. 14 (1963).
9. I.L. Singer and J.S. Murdy, *J. Vac. Sci. Technol.*, **17**(1), 327 (1980).
10. A.G. Hartline, *Met. Trans.*, **5**, 271 (1974).
11. P. Surry, *Br. Corros.*, **13**, 31 (1977).